Coupling and interface effects in magnetic oxide superlattices

2002 J. Phys.: Condens. Matter 14 R947

(http://iopscience.iop.org/0953-8984/14/37/201)

INSTITUTE OF PHYSICS PUBLISHING JOURNAL OF PHYSICS: CONDENSED MATTER

J. Phys.: Condens. Matter **14** (2002) R947–R966 PII: S0953-8984(02)30705-7

TOPICAL REVIEW

Coupling and interface effects in magnetic oxide superlattices

Y Ijiri

Department of Physics and Astronomy, Oberlin College, Oberlin, OH 44074, USA

E-mail: yumi.ijiri@oberlin.edu

Received 18 July 2002
Published 5 September 2002
Online at stacks.iop.org/JPhysCM/14/R947

Abstract

Magnetic oxide superlattices are attractive model systems in which to study coupling and interface effects. After briefly summarizing synthesis and characterization methods, this review describes recent experimental results obtained in investigating epitaxial oxide multilayers comprised primarily of ferromagnetic/paramagnetic, ferromagnetic/antiferromagnetic, and antiferromagnetic/antiferromagnetic materials. The results are discussed in terms of their implications for exchange coupling, exchange biasing, and novel magnetic structures.

(Some figures in this article are in colour only in the electronic version)

1. Introduction

Magnetic multilayer films have been the subject of much intensive research due to their technological use in magnetic recording media and sensors and due to intrinsic interest in the study of coupling mechanisms and finite-size effects [1]. While most of this effort has concentrated on completely metallic layered systems, oxide materials have attracted increasing attention in recent years. In particular, significant work [2, 3] has been done in efforts to understand and expand upon the observations of colossal magnetoresistance (CMR) in perovskite manganite films [4–6] and large tunnelling magnetoresistance (TMR) of oxide barriers [7]. Antiferromagnetic (AF) oxides such as NiO have also been studied increasingly [8, 9], due to their ability to exchange bias or pin the magnetization direction of a neighbouring ferromagnetic (F) layer in a magnetic sensor device [10, 11].

Given this interest in understanding and controlling magnetic oxide thin films, magnetic oxide *superlattices* are particularly attractive as model systems in which to explore the underlying magnetic phenomena. In this subclass of films, two different oxide compounds are grown in alternating layers that still maintain an established epitaxial orientation with respect to one another. The layer thicknesses are of the order of nanometres, so the samples can be viewed as artificial single crystals.

While growth considerations have limited the number and type of systems possible, recent work has illustrated several advantages over more standard polycrystalline films or even ordered bilayer/trilayer films. The superlattices have more controlled interfaces in comparison to polycrystalline counterparts which facilitates comparison to theoretical models. Due to the small individual layer thickness, the magnetic oxide superlattices also have the potential to stabilize magnetic structures not found in bulk form. The multiple repeats highlight interfacial effects and thus provide enhanced magnetic signal for a variety of techniques including standard bulk magnetometry methods and neutron scattering measurements.

This review summarizes the major growth and characterization techniques of magnetic oxide superlattices and highlights results obtained in the past five years in three subclasses comprised of primarily (a) ferromagnetic/(nonmagnetic or paramagnetic), (b) (ferromagnetic or ferrimagnetic)/antiferromagnetic, and (c) antiferromagnetic/(antiferromagnetic of paramagnetic) layers. These classes are of interest in understanding and controlling interlayer coupling, exchange biasing, and interfacial magnetism, respectively. Emphasis is placed on those systems that have generated interest because either they show potential for device application or there is a potential for more detailed comparison to theoretical models.

2. Synthesis and structural characterization

2.1. Synthesis

The synthesis of epitaxial oxide multilayers presents a number of materials challenges. First of all, the two alternating oxide layers must match in crystal structure sufficiently with each other and the substrate in order to maintain a fixed arrangement with respect to one another. Excessive lattice mismatch may lead to a film only textured in a particular orientation or epitaxial only for a very thin total multilayer thickness. Growth conditions must be carefully controlled to avoid composition variations, particularly due to oxide vacancies or intermixing at the interfaces. Reaction rates must also be regulated to prevent the formation of uncorrelated islands and multiple nucleation sites, leading to polycrystalline films.

Given these considerations, one of the most important methods for the synthesis of epitaxial oxide multilayers has been molecular beam epitaxy (MBE) [12]. In this technique, the sample substrate is struck by atomic or molecular beams containing the appropriate elements, sometimes in an easily dissociable precursor form. O_2 or NO_2 gas may be injected or an oxygen plasma may be created to provide the necessary oxygen source. Beam flux rates are carefully controlled, while the growing film quality is usually monitored *in situ*.

MBE methods have been used to create a variety of magnetic oxide superlattices, even ones in which the crystal structures of the two layers are not identical, the strain is significant, or the materials involve ternary oxides.

In particular, MBE superlattices have been constructed with the iron oxide magnetite Fe_3O_4 as one of the layers and intervening layers of a monoxide such as NiO [13], CoO [14, 15], or MgO [16]. As depicted in figure 1, despite the differences in crystal structure between the spinel magnetite and the rock-salt monoxide, the oxygen sublattices match reasonably well, allowing high-quality growth.

In addition, with appropriate care, these methods have allowed growth of layers with a reasonable amount of strain, such as Fe_3O_4/Co_3O_4 superlattices with a 4% mismatch in lattice constants in bulk [17].

As a consequence of the interest in high-temperature superconducting oxides, MBE methods have also been used [18, 19] in the growth of variety of perovskite manganite superlattices with layers of the form $R_{1-x}A_xMnO_3$, where R is a rare-earth and A is an

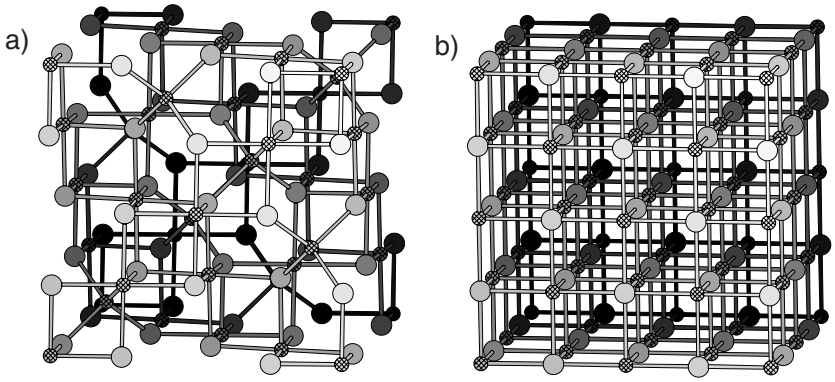

Figure 1. Crystal structures for (a) Fe_3O_4 and (b) MO (where M = Co, Ni), shown slightly canted from a (001) view. In both figures, the larger circles are the oxygen atoms, while the smaller, thatched circles are the metal atoms. Shading indicates depth in the structure. Note the similarities in the oxygen sublattices.

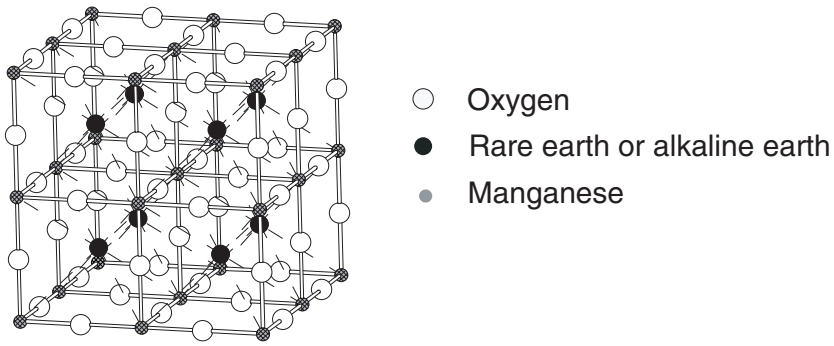

Figure 2. The crystal structure for a cubic perovskite manganite, $R_{1-x}A_xO_3$. Bonds between manganese and oxygen atoms are shown to highlight the Mn environment; dashed lines between manganese and rare-earth/alkaline-earth atoms are shown to indicate placement of the rare earth/alkaline earth in the structure.

alkaline-earth metal as depicted in figure 2. In these superlattices, the usual layer-by-layer growth associated with MBE methods is replaced with a block-by-block approach in which several atomic layers are deposited at a time and then allowed to react to form the desired material. This modification is necessary in order to stabilize the structure, given the cation complexities inherent in these materials.

Pulsed laser deposition (PLD) is another important technique in the formation of epitaxial multilayers [20, 21]. Developed in the late 1980s [22], the method uses a high-energy excimer laser to ablate material from a sintered pellet of a particular compound. The laser wavelength, power, and pulse rate are carefully controlled along with the oxygen pressure and substrate temperature. Reaction rates and local heating effects are of particular concern in the effort to minimize defect formation and interface intermixing problems. On the other hand, the use of preformed targets with the desired compositions greatly simplifies the synthesis process for more complex oxide multilayer films. As a result, this method has been used for producing the majority of the superlattices of the perovskite structure type that will be discussed in the succeeding sections.

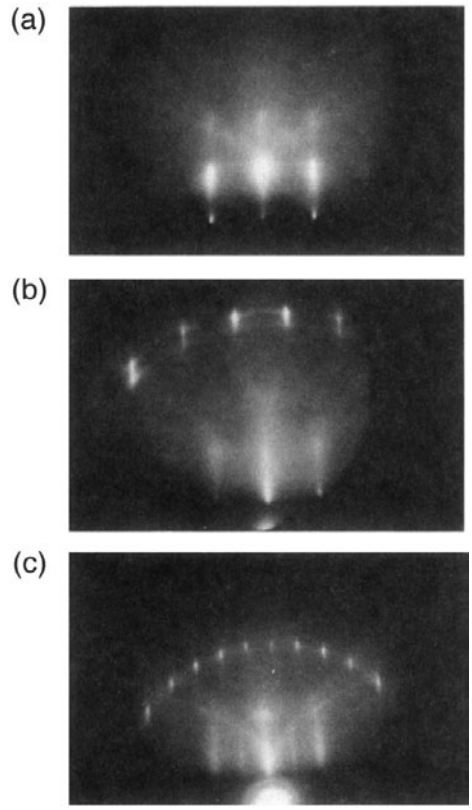

Figure 3. RHEED diffraction images of (a) MgO (001), (b) NiO/MgO (001), and (c) Fe_3O_4/MgO (001), taken along a ⟨100⟩ azimuth. Taken from [13].

Other experimental methods have been used in more limited cases to form magnetic oxide superlattices. For instance, while reactive sputtering usually leads to a distribution of grains, it is possible to use the method to form coherent CoO/NiO multilayers on MgO substrates due to the identical crystal structures and reasonable lattice match of the monoxides [23, 24]. Metal–organic chemical vapour deposition (MOCVD) techniques have also been adapted recently to grow $La_{0.7}Sr_{0.3}MnO_3/SrTiO_3$ superlattices [25]. In MOCVD, precursor materials in the gas phase chemically react to form the desired compound that then grows on the substrate. While the technique is highly versatile in terms of adjusting composition, there are problems with finding appropriate precursors for certain elements, an issue addressed in this case through a controlled pulse delivery of liquid material into the gas phase.

2.2. Structural characterization

As mentioned previously, *in situ* monitoring of the growing film is critical to obtaining high-quality oxide superlattices. By far the most important diagnostic technique during growth is reflection high-energy electron diffraction (RHEED) [26]. In RHEED, a beam of high-energy electrons strikes the sample surface at low angles, and the diffracted beam not only provides phase information but also shows characteristic streaks or spots depending on the size of any islands or steps relative to the electron beam coherence length. Figure 3 illustrates the RHEED patterns for growth of a Fe_3O_4/NiO superlattice.

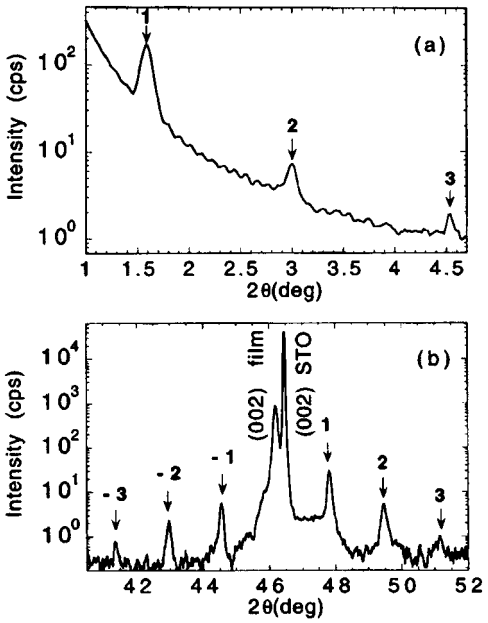

Figure 4. Low-angle (a) and high-angle (b) x-ray data for a $[La_{2/3}Ba_{1/3}MnO_3(47\ Å)/LaNiO_3(15\ Å)]_{12}$ superlattice, illustrating Kiessig fringes and superlattice satellite peaks, respectively. Taken from [28].

After deposition, x-ray scattering methods are typically employed to assess more completely the quality of these superlattices [27]. At low or glancing angles, the x-ray reflectivity is sensitive to variations in refractive index of the multilayers, resulting in intensity oscillations with angle or Kiessig fringes. Figure 4(a) depicts results for a typical $La_{2/3}Ba_{1/3}MnO_3/LaNiO_3$ superlattice [28]. At high angles, θ–2θ and ϕ-scans can be used to determine the Bragg reflections indicative of particular crystal symmetries and phases. Evidence of the superlattice formation can be seen in sidebands or satellite peaks off the major reflections as illustrated in figure 4(b). Simulations of the reflectivity data can be performed to extract layer thicknesses and measures of the extent of interfacial roughness [29].

Two other characterization methods of particular use for oxide superlattices include Rutherford backscattering (RBS) and high-resolution transmission electron microscopy (HRTEM).

In RBS [30], a beam of very high-energy (MeV) ions is incident upon the superlattice, and the number and energy of the backscattered ions at a particular angle are monitored. From these data, information on the composition and thickness of the thin films can be extracted.

In contrast to these more macroscopic assessments of the superlattices, HRTEM has been used often to investigate a small region of the superlattice in more detail. For instance, as shown in figure 5 for a $La_{2/3}Ba_{1/3}MnO_3/SrTiO_3$ superlattice [31], investigations of multilayer cross-sections at high resolution can be used to confirm the registry of atoms from one layer to the next and check for defects or grain formations.

3. Interlayer coupling

Two important issues in understanding the behaviour of thin magnetic films are the effect of layer thickness and the more intrinsic effect of strain. To probe these factors, it is useful

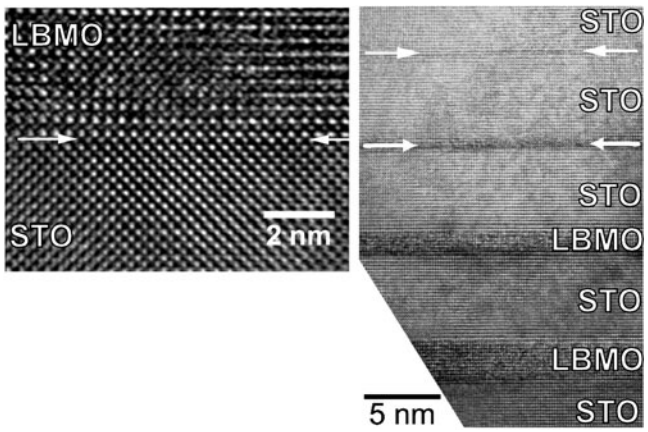

Figure 5. High-resolution TEM images of a $La_{2/3}Ba_{1/3}MnO_3/SrTiO_3$ superlattice. The image on the left illustrates the interface (denoted by arrows) taken in a [010] direction, while the image on the right is taken in the [110] direction. Arrows in the right image indicate the upper two layers of $La_{2/3}Ba_{1/3}MnO_3$. Taken from [31].

to investigate multilayers in which the F layers of interest are separated by intervening nonmagnetic or paramagnetic layers. The multiple repeats increase the signal intensity in magnetization measurements. In the particular case of a superlattice structure, the good control of atomic registry and interface quality regulates the environment for the particular F layers and can be used to alter the associated lattice strain.

These structures are also useful to probe the nature of the interlayer magnetic coupling—in particular, the mechanism(s) by which two F layers influence each other through an intervening nonmagnetic spacer layer. In metallic multilayers, it has been demonstrated that the coupling between two magnetic layers can be either F (parallel) or AF (antiparallel), with an oscillating thickness dependence [32]. The type of coupling has practical implications as well since the particular alignment of successive layers leads to significant differences in the electrical resistance of the multilayer stack [33] due to spin-dependent electron scattering at the interfaces. This so-called giant-magnetoresistive (GMR) effect has been studied extensively for metallic magnetic multilayers and is now used in read heads for magnetic storage media, among other applications [34].

For magnetic oxide superlattices, the majority of the recent work in investigating such strain and coupling effects has focused on perovskite manganite materials of the form $R_{1-x}A_xMnO_3$. These materials are of much interest due to the rediscovery of a phenomenon known as CMR [35] which is particularly large in thin films [4–6]. The resistance of these materials can decrease by many orders of magnitude in an applied magnetic field, as the film or bulk sample undergoes a transition from semiconducting or insulating to metallic behaviour. The class of materials is very robust, since the structure type and its variants support a wide range of different rare-earth and alkaline-earth metals.

Note that in these materials, depending on the ratio of the rare earth R to the alkaline earth A, the manganese has a mixed oxidation state, with both Mn^{3+} and Mn^{4+} sites. In an early explanation of the magnetoresistive (MR) behaviour, Zener [36] recognized the degeneracy of a Mn^{3+}–oxygen–Mn^{4+} and a Mn^{4+}–oxygen–Mn^{3+} configuration and the potential for a 'double-exchange' mechanism connecting the two. With a F alignment of the Mn ions, it is possible for a Mn electron to transfer from the Mn^{3+} to the O^{2-} at the same time as a transfer of an electron from the O^{2-} to the Mn^{4+} site, leading to enhanced conduction.

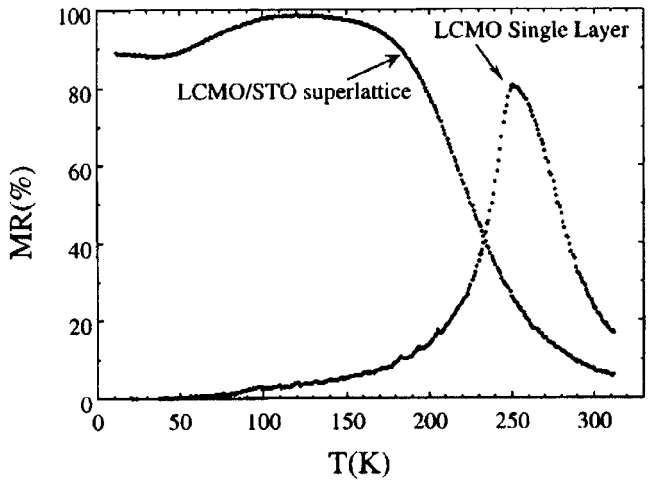

Figure 6. Magnetoresistance percentage at 5 T $((R(0\ \mathrm{T}) - R(5\ \mathrm{T}))/R(0\ \mathrm{T}) \times 100)$ versus temperature for a single layer of $La_{0.7}Ca_{0.3}MnO_3$ and a $La_{0.7}Ca_{0.3}MnO_3$(55 Å)/$SrTiO_3$(160 Å) superlattice. Taken from [39].

While this explanation is central to our current understanding, more recent work [37] has pointed to its quantitative inadequacies, resulting in a renewed interest in studying these materials [38]. In addition, there are a number of challenges in optimizing the MR and TMR behaviour for device applications.

The following subsections outline recent progress in investigating ferromagnetic/nonmagnetic and ferromagnetic/paramagnetic oxide superlattices, primarily of perovskite manganite materials. Section 3.1 concentrates on the role of layer thickness and layer strain in affecting the magnetic behaviour, while section 3.2 describes results more explicitly aimed at probing the interlayer coupling.

3.1. Effects on magnetoresistance and transition temperatures

In analogy to the work on metallic multilayers, much of the recent research on magnetic oxide superlattices has focused on the technological aims of increasing the magnetoresistance in lower applied magnetic fields and more useful temperature ranges for potential recording applications. To do so, a variety of perovskite manganite superlattices have been prepared in which the F layer thickness has been varied.

For instance, Kwon *et al* [39] have demonstrated that relative to a single F film of $La_{0.7}Ca_{0.3}MnO_3$, a $[La_{0.7}Ca_{0.3}MnO_3(55\ \text{Å})/SrTiO_3(160\ \text{Å})]_{20}$ superlattice can have a larger magnetoresistance over a larger temperature range. Specifically, for 0.5 T field relative to zero field, the resistance change of the superlattice was ∼60% versus ∼40% for a single film. The high MR values extended over the temperature range of 10–150 K in comparison to a peak-like structure for a single layer as shown in figure 6.

Jo *et al* [40] have explored this behaviour more systematically with a series of superlattices of the form $[La_{0.7}Ca_{0.3}MnO_3(x)/SrTiO_3(70\ \text{Å})]_y$ with $x = 25$–250 Å and $y = 10$–1 to maintain a constant total F thickness. As a function of decreasing F layer thickness, the peak resistivity temperature T_p showed a decrease, along again with a broadening of the temperature range associated with the metal–insulator transition region and enhanced magnetoresistance. These transport properties were not associated with a significant change in the F ordering temperature

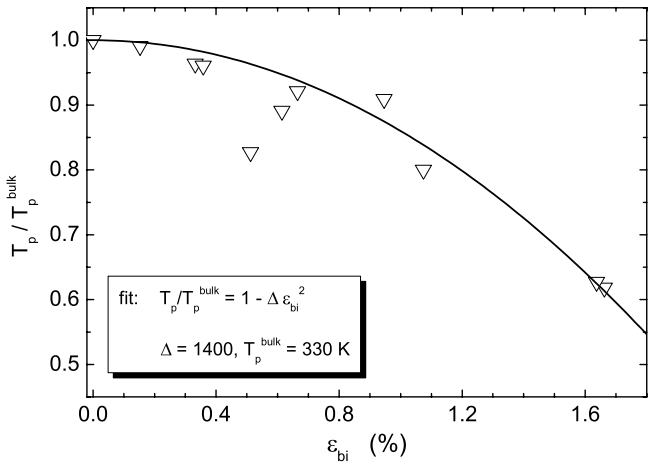

Figure 7. Measured peak resistivity temperature (T_p) normalized against the bulk value (T_p^{bulk}) versus biaxial distortion ε_{bi}. Taken from [31].

($T_C \sim 250$ K) and thus point to a more complicated relationship between the magnetic and transport behaviour.

Analogous effects have been observed in related ferromagnetic/paramagnetic multilayers involving perovskites. Superlattices of $[La_{0.7}Ba_{0.3}MnO_3(x))/SrTiO_3(160\ Å)]_y$ with $x = 54$–540 Å and $y = 20$–2 displayed a similar broadening of the MR transition region as the F layer thickness was reduced [39]. For F $La_{0.6}Pb_{0.4}MnO_3$/paramagnetic $La_{0.85}MnO_{3-\delta}$ superlattices, a maximum MR of 75% was reported at 285 K for 50 Å thick $La_{0.6}Pb_{0.4}MnO_3$ layers in comparison to 25% for a single film of $La_{0.6}Pb_{0.4}MnO_3$ [41].

To understand the origins of these thin-film enhancements to the magnetoresistance, the microstructure of certain superlattices have been investigated in some detail. Using x-ray and HRTEM data, Wiedenhorst *et al* [42] have characterized the strain associated with $La_{2/3}Ba_{1/3}MnO_3$ with $SrTiO_3$ spacers and with $La_{2/3}Sr_{1/3}MnO_3$ also with $SrTiO_3$ spacers. They found that due to a much better lattice match, the barium manganite films remain coherently strained, while the strontium versions segregate for film thicknesses greater than 600 Å into a highly strained and a strain-free region separated by a defect-rich interface. Probing the coherently strained $La_{2/3}Ba_{1/3}MnO_3/SrTiO_3$ superlattices by varying the relative layer thicknesses, they showed (figure 7) that the decrease in T_p and the enhanced magnetoresistance appear well correlated with an increase in biaxial strain, leading to a tetragonal distortion of the $La_{2/3}Ba_{1/3}MnO_3$ layers [31]. More recent work with La–Ca–Mn oxide films has shown that the biaxial strain can lead to a uniaxial metal-to-insulator transition, resulting in superlattices with in-plane metallic and out-of-plane insulating characteristics [43].

In the related $La_{0.5}Sr_{0.5}CoO_3/SrTiO_3$ system, Tanaka and Kawai [44] have found decreases in the F Curie temperatures as a function of decreased layer thickness and increased interfacial strain. This result contrasts with the roughly constant Curie temperatures observed for $La_{0.5}Sr_{0.5}CoO_3/CaTiO_3$ superlattices that were characterized by less strain due to better lattice match.

While a number of these experiments have emphasized the importance of strain in the ability to tailor MR properties, other factors may also contribute significantly. In particular, as discussed in [40] and in [45] for the case of $La_{2/3}Ca_{1/3}MnO_3/Pr_{2/3}Ca_{1/3}MnO_3$ superlattices, interfacial magnetic inhomogeneities or 'dead layers' may lead to large changes in MR behaviour.

In other ferromagnetic/paramagnetic oxide systems, the importance of either the interfacial magnetism and domain structure is very evident. For instance, in yttrium iron garnet (YIG) $Y_3Fe_5O_{12}$ separated by paramagnetic gadolinium gallium garnet $Gd_3Ga_5O_{12}$ layers, changes in the ferrimagnetic resonance and magnetization were understood in terms of the interfacial or surface anisotropy associated with the ultrathin YIG layers [46]. To understand the behaviour of half-metallic Fe_3O_4, MBE-grown superlattices of Fe_3O_4/MgO were investigated, in which part of the Fe_3O_4 layer was doped with Fe^{57} for Mössbauer measurements [47]. These measurements illustrated the significance of the size and width of antiphase boundaries separating domains in determining magnetization properties.

3.2. Nature of interlayer coupling

Instead of focusing on improving the MR properties of oxide superlattices or the properties of individual magnetic layers, other research has concentrated on probing the nature of the coupling between F oxide layers spaced by either paramagnetic or diamagnetic layers.

In a series of papers, Nikolaev *et al* [28, 48, 49] have investigated $[La_{2/3}Ba_{1/3}MnO_3/LaNiO_3]_{10}$ superlattices grown by MBE on $SrTiO_3$ substrates. The thickness of the F lanthanum barium manganite layers was held fixed at 12 unit cells (47 Å), while the paramagnetic lanthanum nickelate layer thickness was varied from 3 to 14 unit cells (11–53 Å).

Investigations of the hysteresis loops have shown that as the thickness of the nickelate spacer layer was decreased, the multilayers had significantly smaller remanent magnetizations and required larger magnetic fields to saturate to the bulk magnetization value of $La_{2/3}Ba_{1/3}MnO_3$ [28, 48]. This behaviour is indicative of AF coupling of successive manganite layers. Studies of the temperature dependence of the magnetization have also shown evidence of the AF coupling for very thin layers ($\sim$11–15 Å). In particular, these oxide superlattices with thin spacer layers showed a *drop* in the magnetization below a characteristic temperature, with very small spontaneous magnetization values in general.

Studying these and related structures as a function of spacer thickness, Nikolaev *et al* [48] have extracted from hysteresis loops values for the coupling strength between successive manganite layers, assuming a coherent rotation of moments upon field reversal. As depicted in figure 8, the coupling was observed to switch from AF to F before dying out. Thus, just like the metallic multilayers [32], these oxide superlattices can display an oscillatory exchange coupling as a function of spacer thickness.

The oscillatory nature and its periodicity are consistent with the predictions of Ruderman–Kittel–Kasuya–Yosida (RKKY) theory, although the strength of the interaction decays quite rapidly. The decay can be accounted for by including a damping parameter due to the electron scattering expected for the nickelate.

The MR behaviour of these $[La_{2/3}Ba_{1/3}MnO_3/LaNiO_3]_{10}$ superlattices reveals additional features of the coupling. As shown in figure 9, the magnetoresistance for superlattices displaying AF coupling (three- or four-unit-cell thickness) is actually *positive* for small magnetic fields, irrespective of field direction relative to current direction. In contrast, for thicker spacer layers, the magnetoresistance curve as a function of applied field is always negative, as is observed in most metallic multilayers. To model this behaviour, Krivorotov *et al* [50] have represented the AF coupling as an additional effective exchange field that acts on each manganite layer, pointing to the interfacial nature of the observed MR.

4. Exchange biasing

Superlattices of F and AF oxides have attracted particular attention recently due to a renewed interest in the phenomenon of *exchange biasing* or *exchange anisotropy* [8, 9]. First discovered

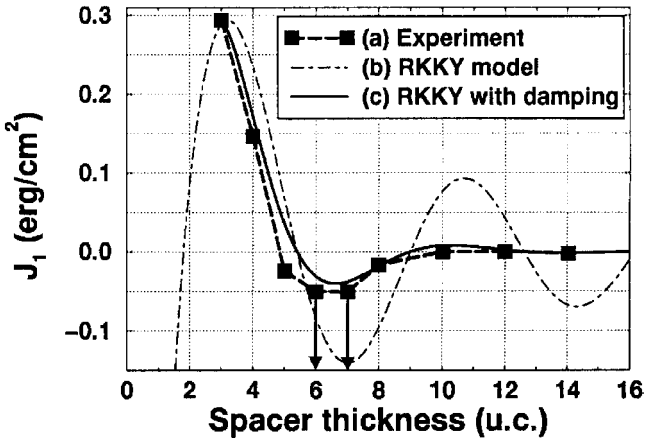

Figure 8. Variation in coupling strength as a function of spacer layer thickness in units of the unit cell. Coupling strength is either taken from experimental hysteresis curves assuming coherent rotation or calculated from a RKKY model with or without damping. Taken from [48].

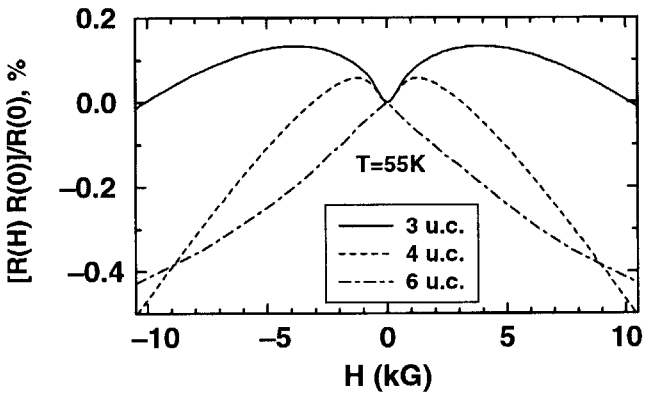

Figure 9. Magnetoresistance (defined as $((R(H) - R(0))/R(0)$ in %) versus in-plane magnetic field for the $[La_{2/3}Ba_{1/3}MnO_3$(12 unit cells)/$LaNiO_3(t)]_{10}$ superlattice. The thickness, t, of the nickelate layer is either 3, 4, or 6 unit cells. Taken from [48].

in the 1950s [51], the effect refers to a *bias* or field shift in the hysteresis loop of a composite system as a result of *exchange* coupling between typically a F and AF material. The bias is usually observed after cooling the F/AF system through the Néel temperature of the AF component. In most early models, this action is presumed to 'lock in' a coupling-induced preferred orientation of the F to the AF spins. As illustrated in figure 10(a), the AF spins at the interface are assumed to have an uncompensated moment that aligns either parallel or antiparallel to the F spins upon cooling. In such a picture, below the Néel temperature, the AF layer is assumed to be frozen in this preferential state. Thus, in order to reverse the F magnetization, an additional applied magnetic field is required, resulting in the observed unidirectional anisotropy.

While this model can describe essential features in the behaviour of Fe/Cr superlattices [52], there are some major difficulties in describing the results for other exchange biasing systems in terms of accounting for the magnitude, temperature dependence, and spin configurations associated with the bias. Other issues include understanding training

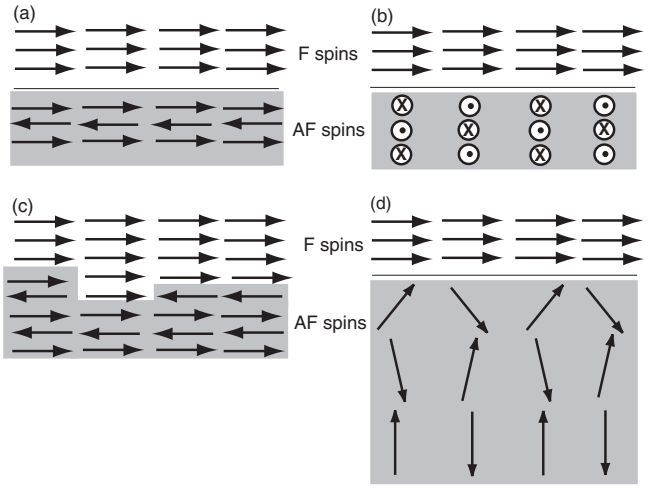

Figure 10. A schematic diagram of several possible arrangements of the F and AF spins assuming (a) a collinear, (b) a perpendicular, (c) a rough, or (d) a canted alignment. The AF spins are indicated in the grey shaded area.

effects and the origins of asymmetry in the hysteresis loop and the often associated coercivity changes. These experimental difficulties have led to a variety of theoretical models [53], which are associated with different spin configurations as depicted partially in figures 10(b)–(d). Thus, despite extensive experimental and theoretical work [8, 9], many questions persist regarding the microscopic mechanisms responsible for the effect. These questions have taken on a technological importance as well, given the use of exchange biased layers in increasing sensitivity to GMR sensors [11].

Because of their high degree of ordering, magnetic oxide superlattices are especially well suited for model studies of exchange biasing. The more controlled interfaces facilitate comparison to theoretical models. The multiple repeats highlights interface effects and in general facilitate magnetization and transport measurements. In addition, the maintenance of structural coherence combined with smooth interfaces allows for characterization by more advanced methods such as neutron diffraction and reflectivity.

The neutron scattering studies are of particular significance in understanding exchange biasing since conventional magnetization methods are relatively insensitive to buried interfaces. This is a difficult problem for AF layers, since the spins of an antiferromagnet alternate directions from site to site, leading to no net magnetization. Other techniques such as x-ray magnetic linear dichroism spectroscopy have also proven useful in measuring the AF spin structure in materials such as NiO [54] although there are important limitations on the thickness of the layers and the applied fields in which an exchange biased sample may be studied. In contrast, neutron scattering methods can be applied in a variety of temperature and field conditions, as the technique is sensitive to the entire sample and to the AF ordering of the spins.

This section focuses first on exchange biased perovskite manganite superlattices. Sections 4.2 and 4.3 then discuss epitaxial superlattices of two exchange biased systems, (1) Fe_3O_4/CoO and (2) Fe_3O_4/NiO, in which substantial characterization of the monoxide AF layer allows for a stronger comparison to theoretical models. In both of these cases, the usual F layer is replaced by magnetite that is *ferrimagnetic*, having moments that alternate in direction but with a net moment remaining.

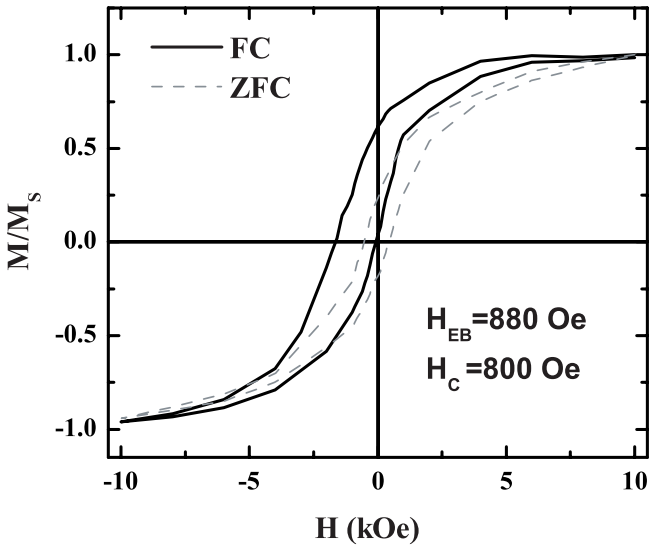

Figure 11. Hysteresis loops at 10 K, taken after cooling in zero field (ZFC) and in 10 kOe (FC) for a $[La_{2/3}Ca_{1/3}MnO_3(50\ Å)/La_{1/3}Ca_{2/3}MnO_3(50\ Å)]_{15}$ superlattice, illustrating an exchange bias field shift of ∼880 Oe and a coercivity of ∼800 Oe. Taken from [55].

4.1. Perovskite manganite superlattices

Superlattices of F and AF perovskite manganites have been of particular recent interest due to the potential for investigating biasing in materials intrinsically unusual as a result of the CMR effect.

One successful example of an exchange biasing perovskite manganite system is the $La_{2/3}Ca_{1/3}MnO_3/La_{1/3}Ca_{2/3}MnO_3$ one. As demonstrated by Panagiotopoulos *et al* [55, 56] and shown in figure 11, superlattices of these two manganite materials exhibited a noticeable field shift in the hysteresis loop as well as an increase in coercivity after field cooling from room temperature. For a variety of different thicknesses of the F or AF manganite layers, the superlattices showed an exponential decay in the size of this bias and coercivity as a function of increasing temperature [57]. These results were interpreted in terms of thermal fluctuations stemming from several potential sources including a spin-glass-like disorder or a distribution of superparamagnetic-like domains.

Several unusual temperature and MR features were noticed for these particular superlattices. The temperature above which biasing is no longer observed is often referred to as the blocking temperature T_B, and for these samples appears at ∼70 K, far from either the bulk Curie temperature of 250 K for the F $La_{2/3}Ca_{1/3}MnO_3$ and from the bulk Néel temperature of 170 K for the AF $La_{1/3}Ca_{2/3}MnO_3$. Unlike in many other systems, however, this value appeared independent of both AF and F layer thickness over a wide range [58]. In addition, the usual transition from insulating to metallic behaviour on decreasing temperature for the F layers was suppressed.

Such features may result from interfacial compositional mixing or other more extrinsic factors in the synthesis of the manganite films, as suggested by Nikolaev *et al* [59]. In investigating $La_{2/3}Ca_{1/3}MnO_3/La_{1/3}Ca_{2/3}MnO_3$ superlattices and trilayers grown by MBE as opposed to PLD, they found that the usual insulating-to-metal transition was still maintained, along with the exchange biasing phenomenon. While their work on biasing in perovskites has

concentrated mostly on trilayers [50, 59], the analysis of the superlattice x-ray diffraction and RBS was useful for obtaining more complete information of the high quality of their interfaces and points to the challenges in analysing these manganite perovskite epitaxial multilayers.

Note that not all F/AF combinations display a discernible bias to the F hysteresis loop, as the spin structures of the two materials must maintain their respective F and AF ordering upon formation of the superlattice. In addition, the antiferromagnet must have sufficient anisotropy and exchange coupling in relation to the ferromagnet in order to influence the F behaviour. For instance, in investigating $La_{0.6}Sr_{0.4}MnO_3/La_{0.6}Sr_{0.4}FeO_3$ superlattices [60], Izumi *et al* did not report on exchange biasing. Instead, they found that as a function of increasing the AF $La_{0.6}Sr_{0.4}FeO_3$ layer thickness, the Curie temperature and magnetization of the F $La_{0.6}Sr_{0.4}MnO_3$ layers were reduced, along with there being an increase in the coercivity. These data combined with resistivity measurements suggested that in response to spin frustration at the interfaces, the manganite layer becomes progressively *AF* with thicker AF ferrite layers. In the related $La_{0.6}Sr_{0.4}MnO_3/La_{0.55}Sr_{0.45}MnO_3$ superlattices [61], exchange biasing was also not observed, as the hysteresis loops for zero-field-cooled and field-cooled superlattices appeared identical. In this system, however, the F $La_{0.6}Sr_{0.4}MnO_3$ and the AF $La_{0.55}Sr_{0.45}MnO_3$ seemed to maintain their respective ordering even for F layers of $\sim$12 Å in thickness. The lack of biasing in this case may stem from insufficient AF anisotropy, either intrinsically or due to the superlattice formation.

4.2. Fe_3O_4/CoO superlattices

Fe_3O_4/CoO superlattices were first grown in the late 1980s by Terashima and Bando [14] and in the 1990s by Wolf *et al* [15]. Initial work on this system has illustrated the presence of an exchange biasing effect for a variety of substrates and even for AF CoO layer thicknesses of down to 5 Å [62]. More recent detailed research has uncovered a number of unusual features, particularly in the alignment of the AF and ferrimagnetic spins, the temperature dependence of the spin arrangements, and the nature of the AF and ferrimagnetic domains [63–65]. These features place important constraints on appropriate models for exchange biasing and illustrate the complexity of the phenomenon.

As in the bulk, the CoO in the superlattices ordered antiferromagnetically, with planes of spins that alternate in $\langle 111 \rangle$ propagation directions. However, unlike the case for bulk CoO, neutron diffraction measurements showed that the specific Co spin axes were altered to either [110] or $[1\bar{1}0]$ directions that lie within the sample growth plane, as shown in figure 12. The cobalt oxide anisotropy was so strong that changes in the Fe_3O_4 moment directions and high magnetic fields ($\sim$5 T) resulted not in changes of the Co spin axes, but rather in a redistribution of the AF spins into $\{111\}$ domains with either [110] or $[1\bar{1}0]$ directions.

The coupling between the Fe_3O_4 and CoO layers was very evident in experiments with different applied magnetic fields. In contrast to early models [51], the observed alignment of the CoO spins relative to the Fe_3O_4 spins was preferentially into domains that are *perpendicular*, not collinear, to the magnetite [63, 64]. In samples exhibiting the most prominent exchange biasing characteristics (largest field shifts at highest temperatures), memory of the original field direction was retained unless high-temperature cycling of the magnetic field was conducted to randomize the Fe_3O_4 domains. Such spin alignment is consistent with several theoretical predictions [66, 67] as well as other systems [68] in which perpendicular coupling has been observed. However, there has been significant theoretical discussion as to what the nature of the spins must be (constrained or 3D Heisenberg for instance) in order to lead to biasing [69].

The temperature onset of coherent, long-range ordering was also altered in these superlattices from the bulk Curie temperature $T_C \sim 858$ K for magnetite [70] and the bulk

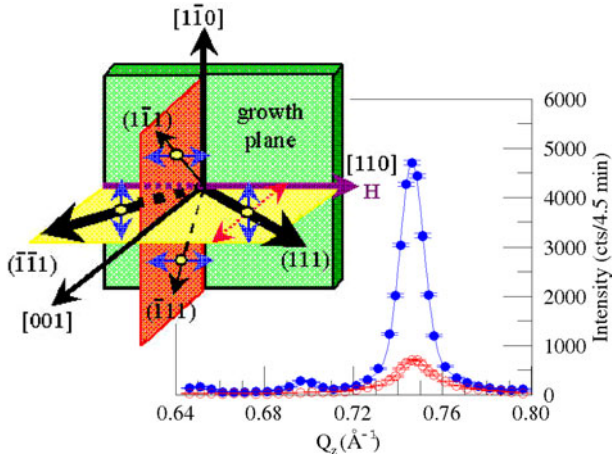

Figure 12. Co spin directions for Fe_3O_4/CoO superlattices, along with supporting neutron scattering data from which directions were determined. Taken from [63].

Néel temperature $T_N \sim 291$ K for cobalt oxide [71]. As shown in figure 13, the CoO effective ordering or Néel temperature was enhanced from a slightly elevated, but bulk-like, ordering temperature of $\sim 325 \pm 15$ K for 100 Å CoO layers to even higher temperatures of $\sim 510 \pm 10$ K for 17 Å CoO layers. The enhancement of the ordering temperature for thinner CoO layers relative to Fe_3O_4 ones is consistent with a mean-field picture in which the ordering temperatures of the two disparate elements approach each other as the relative concentration is varied. More rigorously, the changes in the ordering behaviour can be modelled using Monte Carlo calculations based on an appropriate Heisenberg Hamiltonian [72]. These calculations are sensitive to the nature of the interface spins and suggest a complex interplay between domain size and ordering behaviour.

The changes in the onset of long-range order contrast with the temperature dependence of the exchange biasing itself [65]. In a simple picture of exchange biasing, T_B is identical to the ordering temperature of the antiferromagnet, T_N, since it is the antiferromagnet that 'locks in' the biasing. However, as depicted in figure 13 and observed in a number of other exchange biased systems [73–75], the blocking temperature decreased with decreasing CoO thickness. While this behaviour is sometimes attributed to finite-size effects suppressing the AF ordering temperature, this is clearly incorrect for these superlattices in which *lower* blocking temperatures for thinner CoO layers contrasted with *higher* AF ordering temperatures. Instead, the T_Bs were associated with the temperatures at which the preference for perpendicular coupling of the CoO and Fe_3O_4 began to freeze in.

The Fe_3O_4/CoO superlattices exhibited several interesting features as regards domain structures. Note that since the intervening CoO structure is simpler than the Fe_3O_4 one, there is no unique alignment of successive Fe_3O_4 layers relative to each other. This ambiguity in stacking limits the growth axis coherence length of the Fe_3O_4 layers to the thickness of a single layer, while the in-plane size can be factors of two or three greater. The structure of such domains has been of particular interest in recent years, due to experiments investigating the role of antiphase boundaries in magnetite films [76]. The CoO domain structure is even more unusual in these superlattices. Due to the ferrimagnetic nature of the Fe_3O_4, the CoO AF ordering can persist through intervening Fe_3O_4 layers, resulting in growth axis coherence lengths that extend from one CoO layer to the next. These relatively large domains (of order $\sim$300–1000 Å) contrast with the typical sizes (30–100 Å) observed for polycrystalline grains.

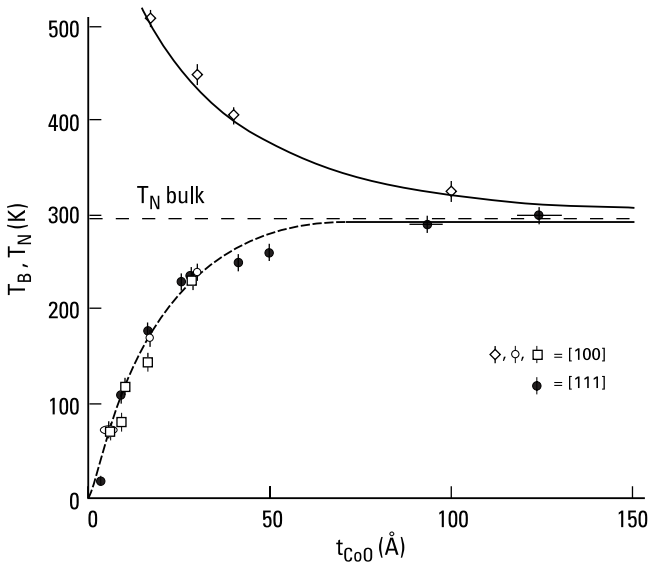

Figure 13. Measured CoO ordering temperatures (T_N) and blocking temperatures (T_B) versus thickness of the CoO layer for the Fe_3O_4/CoO system. Symbols denote different directions of growth on the substrate. Taken from [65].

In investigating the behaviour of these domains as a function of different exchange biasing conditions, Ijiri *et al* [64] have observed that both the ferrimagnetic and coupling-favoured AF domains grew on cooling in an applied magnetic field. Subsequent field cycling, however, resulted in little change to the average domain sizes. Such frozen behaviour is consistent with the predictions of a subset of proposed theoretical models of biasing [69, 77], although significant modifications are necessary to also account for the observed spin structures.

4.3. Fe_3O_4/NiO superlattices

Fe_3O_4/NiO superlattices have been grown extensively by Lind *et al*, beginning in the early 1990s [13]. Like their Fe_3O_4/CoO counterparts, the NiO-containing superlattices exhibited exchange biasing features associated with different spin structures and domain characteristics.

As part of thin-layer superlattices, the NiO components retained some features of the bulk, but with several important modifications. In bulk, the antiferromagnet NiO adopts a similar structure to CoO, with planes of spins alternating in ⟨111⟩ directions but with a significantly weaker magnetocrystalline anisotropy along with a higher ordering temperature of 520 K versus 291 K [78]. This high T_N for bulk has made NiO a candidate for providing better thermal stability in sensor applications [79], although less convenient for laboratory investigations of temperature effects. For the superlattices, neutron diffraction measurements have shown that the AF NiO layers retained the {111} domain structure along with bulk-like anisotropy axes, but with ordering temperatures again elevated as a result of coupling to the high-ordering Fe_3O_4 layers [80].

The coupling of the NiO spins to the Fe_3O_4 layers was more complicated than that observed for the Fe_3O_4/CoO superlattices. While a number of the Ni spins preferentially aligned perpendicular to the ferrimagnetic Fe spins, a significant fraction of the Ni spins appeared to disorder at high magnetic fields [81]. Thus, it is less clear in this system what is the nature of the spin structures associated with exchange biasing.

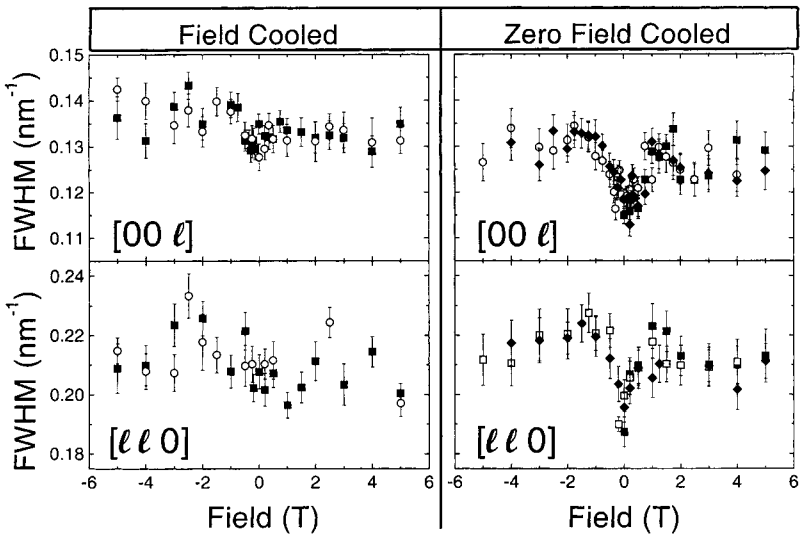

Figure 14. Neutron diffraction data on the full width at half-maximum (FWHM) of the (111) NiO reflection as a function of field after cooling from room temperature in a 5 T field or cooling in zero field for a $[Fe_3O_4(60\ Å)/NiO(110\ Å)]_{100}$ superlattice. The plots show the FWHM for scans either along the growth axis direction [00l] or within the sample plane [*ll*0]. Symbols indicate data from separate cycles of the applied magnetic field. Taken from [81].

However, investigations of the overall domain structures in Fe_3O_4/NiO superlattices have revealed several interesting features connected with biasing. Polarized neutron reflectivity experiments have uncovered asymmetries in the depth-dependent magnetization associated with the iron oxide layers [82]. In particular, for exchange biased samples, the Fe_3O_4 saturation magnetization in the field-cooled direction was inequivalent to that in the reversed direction, suggestive of the formation of domain walls. More recently, experiments probing the AF domains have shown field dependences of the domain size that were correlated with the presence or absence of exchange biasing [81]. Figure 14 displays information on the peak width of an AF domain that after instrument resolution corrections is inversely related to the average AF domain size. As depicted in the figure, the average AF domain sizes both in the plane and along the growth axis in field-cooled, biased superlattices were insensitive to subsequent field cyclings, while for unbiased superlattices, these domain sizes changed with field, particularly at values corresponding to the coercivities of the Fe_3O_4 layers. Thus, as in the case of the Fe_3O_4/CoO superlattices, the exchange biasing for NiO layers was associated with frozen AF domains.

5. Novel interfacial magnetic structures

Another potential use for magnetic oxide superlattices is to create unusual magnetic structures not easily stabilized in bulk form, as a result of the constraint of the substrate and the thin layers of the two superlattice materials. In addition to having novel spin arrangements, such multilayers can also serve as tests for theoretical predictions of the expected magnetism. It is of particular interest to investigate superlattices comprised of two different AF or paramagnetic (PM) oxides. Since neither AF nor paramagnetic materials have a net magnetization in zero field, the observation of any appreciable magnetic signal in AF/AF or AF/PM multilayers

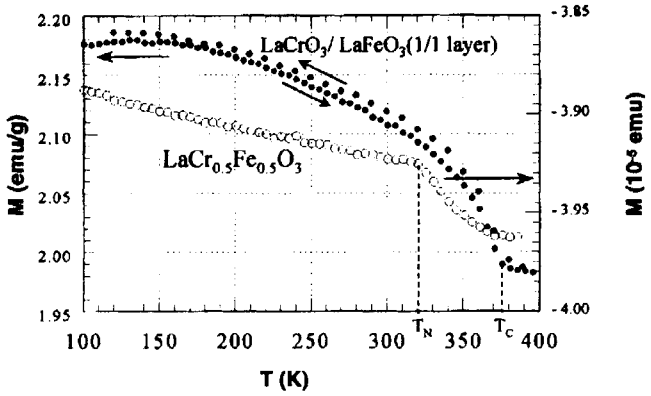

Figure 15. Magnetization versus temperature for a $LaCrO_3$(2.3 Å)/$LaFeO_3$(2.3 Å) superlattice and a solid solution of $LaCr_{0.5}Fe_{0.5}O_3$. Taken from [86].

can be a clear signature for a possible interface-induced ferromagnetism. In the following subsections, we describe recent results reported on two different perovskite oxide systems, namely $LaFeO_3$/$LaCrO_3$ and $CaMnO_3$/$CaRuO_3$ superlattices, although others such as the $LaMnO_3$/$SrMnO_3$ system have also been investigated in an analogous fashion [83].

5.1. $LaFeO_3$/$LaCrO_3$ superlattices

$LaFeO_3$ and $LaCrO_3$ are well-known AF oxides of the perovskite structure type. In general, the magnetic ordering in these oxides is well described by the superexchange interaction in which the moments on metal cations couple via intervening oxygen atoms [84]. Considering such an interaction and the structure of both $LaFeO_3$ and $LaCrO_3$, it is expected that while the Fe–O–Fe and Cr–O–Cr interactions generate AF coupling, Fe–O–Cr coupling should lead to ferromagnetism [85].

However, early attempts to prepare polycrystalline versions of La(Fe–Cr)O_3 have often resulted in either phase-separated mixtures of the two oxides or randomly distributed mixtures of Fe and Cr ions—neither of which showed appreciable F properties, as the AF coupling predominated. In contrast, through the use of PLD with its interfacial control, Ueda *et al* [86] have demonstrated that it is possible to achieve F ordering in $LaFeO_3$/$LaCrO_3$ superlattices under certain circumstances.

As illustrated in figure 15, the magnetization versus temperature for a $LaFeO_3$(2.3 Å)/La CrO_3(2.3 Å) superlattice grown on $SrTiO_3$(111) showed the typical magnitude and shape expected for ferromagnetism with a T_C of ∼375 K and a moment per site of ∼3 μ_B. At temperatures below T_C, magnetization versus applied field curves also displayed noticeable hysteresis and remanent magnetization. In contrast, a solid solution of $LaFe_{0.5}Cr_{0.5}O_3$ had a magnetization many orders of magnitude lower, with a cusp consistent with the onset of AF ordering at ∼ 320 K.

Note that the observation of ferromagnetism in this system was highly dependent on the manner in which the growth was regulated. While $LaFeO_3$/$LaCrO_3$ superlattices on (111) $SrTiO_3$ had F properties, growth on (100) and (110) $SrTiO_3$ instead preserved AF characteristics, but with changes to the appropriate Néel temperatures [87]. These results were consistent with the expected Fe–O–Fe, Fe–O–Cr, and Cr–O–Cr interactions for growth in different directions.

5.2. $CaMnO_3/CaRuO_3$ superlattices

The $CaMnO_3/CaRuO_3$ system offers another opportunity to investigate the formation of artificially constructed F ordering. While $CaMnO_3$ is an antiferromagnet with $T_N \sim 123$ K and $CaRuO_3$ is paramagnetic or weakly AF, a substantial portion of the solid-solution range for $CaMn_{1-x}Ru_xO_3$ displays F properties. However, as discussed by Maignan *et al* [88], the polycrystalline samples appear to have inhomogeneous magnetic states, with superexchange interactions between Mn and Ru and different valencies for the Mn and Ru ions over the substitution range most probably responsible for the observed magnetic properties. To elucidate further the nature of the magnetism, it is of great interest to investigate multilayers in which the structure is controlled better.

Recently, Takahashi *et al* [89] have synthesized a series of $[CaMnO_3/CaRuO_3]_{15}$ superlattices with the manganite layer thickness held fixed at 10 unit cells and the ruthenate layer thickness varied from 2 to 10 unit cells. In each case, the superlattices showed F behaviour with almost identical transition temperatures T_C of $\sim$95 K, in contrast to the range observed in polycrystalline samples. The magnetization per interface Mn/Ru ion was also constant, indicating that the ferromagnetism was associated with the interfaces and not throughout the structure. In addition, while the conduction scaled with the ruthenate thickness, the change in resistance with field did not vary as strongly. These results were consistent with a picture in which conduction occurs mainly through the ruthenate layers, with modifications due to only the interfacial manganese–ruthenium ions.

6. Conclusions

As described in this review, recent research into magnetic oxide superlattices has explored a number of interesting coupling and interface effects. Due to the interfacial and structural control, studies of these ordered multilayers have provided a more complete picture of exchange coupling, exchange biasing, and interface ferromagnetism than is possible with polycrystalline counterparts. While the work here has focused on superlattices of F/PM, F/AF, and AF/AF oxides, a wide variety of magnetic states can be formed by combining ferromagnetic or ferrimagnetic oxides as well, to obtain enhanced magnetoresistance [90, 91] or unusual compensation points and phase transitions [92]. Given the growing interest in magnetic oxides for sensors and other devices, it is likely that studies of all of these superlattices will be of much importance in the years to come.

Acknowledgments

This work was supported in part by the ACS Petroleum Research Fund. The author acknowledges collaborations and fruitful discussions with J A Borchers, R W Erwin, D M Lind and P J van der Zaag.

References

[1] Grunberg P 2001 *J. Phys.: Condens. Matter* **13** 7691
[2] Compare
Mercey B, Wolfman J and Raveau B 1999 *Curr. Opin. Solid State Mater. Sci.* **4** 24 and references therein
[3] Compare
Prellier W, Lecoeur Ph and Mercey B 2001 *J. Phys.: Condens. Matter* **13** 915 and references therein
[4] Jin S, Tiefel T H, McCormack M, Fastnacht R A, Ramesh R and Chen L H 1993 *Science* **264** 413
[5] von Helmolt R, Wecker J, Holzapfel B, Schultz L and Samwer K 1993 *Phys. Rev. Lett.* **71** 2331

[6] Chahara K, Ohno T, Kasai M and Kozono Y 1990 *Appl. Phys. Lett.* **63**
[7] Moodera J S, Kinder L R, Wong T M and Meservey R 1995 *Phys. Rev. Lett.* **74** 3273
[8] Compare
Nogues J and Schuller I 1999 *J. Magn. Magn. Mater.* **192** 203 and references therein
[9] Compare
Berkowitz A E and Takano K 1999 *J. Magn. Magn. Mater.* **200** 552 and references therein
[10] Lin T, Tsang C, Fontana R E and Howard J K 1985 *IEEE Trans. Magn.* **31** 2585
[11] Dieny B, Speriosu V S, Parkin S S P, Gurney B A, Wilhoit D R and Mauri D 1991 *Phys. Rev.* B **43** 1297
[12] Compare
Chamber S A 2000 *Surf. Sci. Rep.* **39** 105 and references therein
[13] Lind D M, Berry S D, Chern G, Mathias H and Testardi L R 1992 *Phys. Rev.* B **45** 1838
[14] Terashima T and Bando Y 1987 *Thin Solid Films* **152** 455
[15] Wolf R M, De Veirman A E M, van der Sluis P, van der Zaag P J and ann de Stegge J B F 1994 *Mater. Res. Soc. Symp. Proc.* **341** 23
[16] James M A, Voogt F C, Niesen L, Rogojanu O C and Hibma T 1998 *Surf. Sci.* **402–404** 332
[17] Sohma M, Kawaguchi K and Manago T 2001 *J. Appl. Phys.* **89** 2843
[18] Achutharaman V S, Beauchamp K M, Chandrasekhar N, Spalding G C, Johnson B R and Goldman A M 1992 *Thin Solid Films* **216** 14
[19] Locquet J P, Catana A, Machler A E, Gerber C and Bednorz J G 1994 *Appl. Phys. Lett.* **64** 372
[20] Saenger K L 1993 *Process. Adv. Mater.* **3** 1
Saenger K L 1993 *Process. Adv. Mater.* **3** 63
[21] Chrisey D B and Hubler G K 1994 *Pulsed Laser Deposition of Thin Films* (New York: Wiley)
[22] Dijkkamp D, Venkatesan T, Wu X D, Shaheen S A, Jisrawi N, Min-Lee Y H, McLean W L and Croft M 1987 *Appl. Phys. Lett.* **51** 619
[23] Carey M J, Spada F E, Berkowitz A E, Cao W and Thomas G 1991 *J. Mater. Res.* **6** 2680
[24] Borchers J A, Carey M J, Erwin R W, Majkrzak C F and Berkowitz A E 1993 *Phys. Rev. Lett.* **70** 1878
[25] Dubourdieu C, Rosina M, Weiss F, Sénateur J P and Hodeau J L 2001 *Appl. Phys. Lett.* **79** 1246
[26] Mahan J E, Geib K M, Robinson G Y and Long R G 1990 *J. Vac. Sci. Technol.* A **8** 3692
[27] Fewster P F 1996 *Rep. Prog. Phys.* **59** 1339
[28] Nikolaev K R, Bhattacharya A, Kraus P A, Vas'ko V A, Cooley W K and Goldman A M 1999 *Appl. Phys. Lett.* **75** 118
[29] Chason E and Mayer T M 1997 *Crit. Rev. Solid State Mater. Sci.* **22** 1
[30] Lieb K P 1999 *Contemp. Phys.* **40** 385
[31] Lu Y, Klein J, Wiedenhorst B, Philipp J B, Herbstritt F, Marx A, Alff L and Gross R 2000 *Phys. Rev.* B **62** 15 806
[32] Parkin S S P, More N and Roche K P 1990 *Phys. Rev. Lett.* **64** 2304
[33] Baibich M N, Broto J M, Fert A, Nguyen V D, Petroff F, Eitenne P, Creuzet G, Friederich A and Chazelas J 1988 *Phys. Rev. Lett.* **61** 2472
[34] Daughton J M, Pohm A V, Fayfield R T and Smith C H 1999 *J. Phys. D: Appl. Phys.* **32** R169
[35] van Santen J H and Jonker G 1950 *Physica* **16** 599
[36] Zener C 1951 *Phys. Rev.* **2** 403
[37] Millis A, Littlewood P and Shraiman B I 1995 *Phys. Rev. Lett.* **74** 5144
[38] Compare
Salamon M B and Jaime M 2001 *Rev. Mod. Phys.* **73** 583 and references therein
[39] Kwon C, Kim K-C, Robson M C, Gu J Y, Rajeswari M, Venkatesan T and Ramesh R 1997 *J. Appl. Phys.* **81** 4950
[40] Jo M-H, Mathur N D, Evetts J E, Blamire M G, Bibes M and Fontcuberta J 1999 *Appl. Phys. Lett.* **75** 3689
[41] Sahana M, Hegde M S, Prasad V and Subramanyam S V 1999 *J. Appl. Phys.* **85** 1058
[42] Wiedenhorst B, Höfener C, Lu Y, Klein J, Alff L, Gross R, Freitag B H and Mader W 1999 *Appl. Phys. Lett.* **74** 3636
[43] Alff L 2002 private communication
[44] Tanaka H and Kawai T 1999 *Phys. Rev.* B **60** 14 163
[45] Li H, Sun J R and Wong H K 2002 *Appl. Phys. Lett.* **80** 628
[46] Chern M Y, Fang C C, Liaw J S, Lin J G and Huang C Y 1996 *Appl. Phys. Lett.* **69** 854
[47] Strijkers G J, Kohlhepp J T, van der Heijden P A A, Swagten H J M and Gaines J M 1999 *J. Appl. Phys.* **85** 5294
[48] Nikolaev K R, Dobin A Yu, Krivorotov I N, Cooley W K, Bhattacharya A, Kobrinskii A L, Glazman L I, Wentzovitch R M, Dahlberg E D and Goldman A M 2000 *Phys. Rev. Lett.* **85** 3728

[49] Nikolaev K R, Dobin A Yu, Krivorotov I N, Dahlberg E D and Goldman A M 2001 *J. Appl. Phys.* **89** 6820
[50] Krivorotov I N, Nikolaev K R, Dobin A Yu, Goldman A M and Dahlberg E D 2001 *Phys. Rev. Lett.* **86** 5779
[51] Meiklejohn W H and Bean C P 1956 *Phys. Rev.* **102** 1413
Meiklejohn W H and Bean C P 1957 *Phys. Rev.* **105** 904
[52] Jiang J S, Felcher G P, Inomata A, Goyette R, Nelson C and Bader S D 2000 *Phys. Rev.* B **61** 9653
[53] Compare
Kiwi M 2001 *J. Magn. Magn. Mater.* **234** 584 and references therein
[54] Ohldag H, Scholl A, Nolting F, Anders S, Hillebrecht F U and Stöhr J 2001 *Phys. Rev. Lett.* **86** 2878
[55] Panagiotopoulos I, Christides C, Moutis N, Pissas M and Niarchos D 1999 *J. Appl. Phys.* **85** 4913
[56] Panagiotopoulos I, Christides C, Pissas M and Niarchos D 1999 *Phys. Rev.* B **60** 485
[57] Moutis N, Christides C, Panagiotopoulos I and Niarchos D 2001 *Phys. Rev.* B **64** 094429
[58] Panagiotopoulos I, Christides C, Niarchos D and Pissas M 2000 *J. Appl. Phys.* **87** 3926
[59] Nikolaev K R, Krivorotov I N, Cooley W K, Bhattacharya A, Dahlberg E D and Goldman A M 2000 *Appl. Phys. Lett.* **76** 478
[60] Izumi M, Murakami Y, Konishi Y, Manako T, Kawasaki M and Tokura Y 1999 *Phys. Rev.* **60** 1211
[61] Izumi M, Manako T, Konishi Y, Kawasaki M and Tokura Y 2000 *Phys. Rev.* B **61** 12 187
[62] van der Zaag P J, Ball A R, Feiner L F, Wolf R M and van der Heijden P A A 1996 *J. Appl. Phys.* **79** 5103
[63] Ijiri Y, Borchers J A, Erwin R W, Lee S H, van der Zaag P J and Wolf R M 1998 *Phys. Rev. Lett.* **80** 608
[64] Ijiri Y, Borchers J A, Erwin R W, Lee S H, van der Zaag P J and Wolf R M 1998 *J. Appl. Phys.* **83** 6882
[65] van der Zaag P J, Ijiri Y, Borchers J A, Feiner L F, Wolf R M, Gaines J M, Erwin R W and Verheijen M A 2000 *Phys. Rev. Lett.* **84** 6102
[66] Hinchey L L and Mills D L 1986 *Phys. Rev.* B **34** 1689
[67] Koon N C 1997 *Phys. Rev. Lett.* **78** 4865
[68] Moran T J, Nogues J, Lederman D and Schuller I K 1998 *Appl. Phys. Lett.* **72** 617
[69] Schulthess T C and Butler W 1998 *Phys. Rev. Lett.* **81** 4516
Schulthess T C 2002 private communication
[70] Shull C G, Wollan E O and Koehler W C 1951 *Phys. Rev.* **84** 912
[71] Roth W L 1958 *Phys. Rev.* **110** 1333
[72] Tsai S-H, Landau D P and Schulthess T C 2002 *J. Appl. Phys.* **91** 6884
[73] Parkin S S P and Speriosu V S 1990 *Springer Proc. Phys.* **50** 110
[74] Ambrose T and Chien C L 1998 *J. Appl. Phys.* **83** 6822
[75] Devasahayam A J and Kryder M H 1999 *J. Appl. Phys.* **85** 5519
[76] Margulies D T, Parker F T, Rudee M L, Spada F E, Chapman J N, Aitchison P R and Berkowitz A E 1997 *Phys. Rev. Lett.* **79** 5162
[77] Malozemoff A P 1988 *J. Appl. Phys.* **63** 3874
[78] Roth W L 1960 *J. Appl. Phys.* **31**
[79] Carey M J, Smith N, Gurney B A, Childress J R and Lin T 2001 *J. Appl. Phys.* 6579
[80] Borchers J A, Erwin R W, Berry S D, Lind D M, Ankner J F, Lochner E, Shaw K A and Hilton D 1995 *Phys. Rev.* B **51** 8276
[81] Borchers J A, Ijiri Y, Lind D M, Ivanov P G, Erwin R W, Qasba A, Lee S-H, O'Donovan K V and Dender D C 2000 *Appl. Phys. Lett.* **77** 4187
[82] Ball A R, Leenaers A J G, van der Zaag P J, Shaw K A, Singer B, Lind D M, Frederikze H and Rekveldt M Th 1996 *Appl. Phys. Lett.* **69** 1489
[83] Salvador P A, Haghiri-Gosnet A M, Mercey B, Hervieu M and Raveau B 1999 *Appl. Phys. Lett.* **75** 2638
[84] Anderson P W 1950 *Phys. Rev.* **79** 350
[85] Kanamori J 1959 *J. Phys. Chem. Solids* **10** 87
[86] Ueda K, Tabata H and Kawai T 1998 *Science* **280** 1064
[87] Ueda K, Tabata H and Kawai T 2001 *J. Appl. Phys.* **89** 2847
[88] Maignan A, Martin C, Hervieu M and Raveau B 2001 *Solid State Commun.* **117** 377
[89] Takahashi K S, Kawasaki M and Tokura Y 2001 *Appl. Phys. Lett.* **79** 1324
[90] Gong G Q, Gupta A, Xiao G, Lecoeur P and McGuire T R 1996 *Phys. Rev.* B **54** 3742
[91] Pietambaram S V, Kumar D, Singh R K and Lee C B 2001 *Appl. Phys. Lett.* **78** 243
[92] Chern G, Horng L, Shieh W K and Wu T C 2001 *Phys. Rev.* B **63** 094421